

# Sound transmission of periodic composite structure lined with porous core: rib-stiffened double panel case

Hou Qiao<sup>a</sup>, Zeng He<sup>a,b,\*</sup>, Wen Jiang<sup>a,b</sup>, Weicai Peng<sup>c</sup>

<sup>a</sup>*Department of Mechanics, Huazhong University of Science & Technology, Wuhan, China*

<sup>b</sup>*Hubei Key Laboratory for Engineering Structural Analysis and Safety Assessment, Huazhong University of Science & Technology, Wuhan, China*

<sup>c</sup>*National Key Laboratory on Ship Vibration and Noise, China Ship Development and Design Center, Wuhan, China*

---

## Abstract

This paper develops a modeling procedure combining Biot theory and space harmonic series for the one-dimensional periodic composite structure with porous lining. The periodically rib-stiffened case is discussed to illustrate the proposed method. Detailed solution procedures are shown using the bonded-bonded boundary case. The modeling procedure is validated using theoretical and finite element method results. The influence of modeling parameters is studied. Qualitative results are obtained. Despite the cumbersome truncation, the method here can be promising in broadband sound modulation by combining the poroelastic modeling and periodic structures semi-analytically.

*Keywords:* Sound transmission; Periodic composite structure; Porous media; rib-stiffened double panel; space harmonic series

---

## 1. Introduction

Due to the high stiffness to weight ratio, multi-panel structures are widely used in engineering applications, such as aircraft, underwater and building structures. Their acoustic performance is studied for a long time.

Composite multi-panel structures without any attachments or fillings are always the simplest case. Concerning their sound transmission loss (STL), both theoretical, experimental and numerical methods are employed. Xin and Lu [1] and Sakagami [2] are representatives of theoretical models; experimental results are included in the latter. Semi-empirical models are also used, the representatives are the models by Sharp [3] and Gu [4], improved models by Davy [5]; the prediction models are reviewed and compared by Hongisto [6] and Legault [7] contemporarily. No theoretical or semi-empirical model appropriate for the case studied here though.

Much more attention is paid to the composite multi-panel structure with attachments or absorption fillings. The absorption fillings are complicated; nonetheless, they can be

---

\*Corresponding author

*Email address:* hz@mail.hust.edu.cn (Zeng He)

considered as porous materials in most cases, thus the models of porous media can be utilized. Two widely used theoretical models for porous media are the Biot theory [8] and the equivalent fluid model (EFM) [9].

The EFM is widely used together with some numerical or semi-analytical treatment due to its simplicity. Double partition structures with porous cavity were studied by EFM [10], or together with semi-analytical method [11]. Liu [12] used EFM together with the transfer matrix method (TMM), utilizing the simplification by Lee [13]; the formulation was different from Xin [11]. STL of double panel structures filled with fiberglass was studied by Legault and Atalla, using EFM together with finite element method (FEM) [14] or experiments [7].

When it comes to elastic frame porous media, the EFM is invalid and the Biot theory [8] should be used. Two-dimensional (2D) poroelastic field variables within porous media are given by Bolton [15] using the Biot theory; the simplifications of Deresiewicz [16] and Allard [17] are adopted. This 2D model was extended to the three-dimensional (3D) case by Zhou [18]. Liu [19] investigated the effects of flow on the multi-panel structures using the 3D model. Numerical methods [20] were also developed based on the Biot theory.

Meanwhile, multi-panel structures with attachments were prominent too. The current study is mainly about those with ribs, resilient mountings or elastic coatings; while the absorption fillings are absent. One of the most useful methods for these problems is the space harmonic series (SHS) introduced by Mead and Pujara [21]; it is still useful for periodic structures today. Utilizing the SHS, Xin studied the STL of rib-stiffened sandwich structures [22]; Legault and Atalla investigated the effects of structure links [7] and resilient mountings [14] on the STL of double panel structures. The drawback of the SHS is illustrated by Legault [23]. The Fourier transform method (FTM) [24] is also useful for these periodic problems. Using the FTM, multi-panel structures were investigated by Lin [25] and Brunskog [26]; Xin [11] studied these structures with absorption fillings together with EFM. In fact, the same nature is shared between FTM and SHS as pointed out by Mace [24]. Another useful method for these structures is the modal approach. Using the orthonormal modal functions, the vibration [27], structural intensity [28], and modal characteristics [29] of simply supported ribbed structures were studied. For double panel structures, the work of Xin [30] and Liu [31] can be representatives. However, for porous media, relevant orthonormal modal functions are not available for now.

Despite the fruitful research conducted on multi-panel structures, there are few papers on those with both periodic boundary and the porous core, or try to solve these problems using the Biot theory. For example, Xin [11] and Legault [7, 14] all studied these periodic multi-panel structures using EFM. Inspired by Bolton [15] and Zhou [18], the poroelastic field with periodic boundary conditions is deduced here utilizing the Biot theory and SHS; then the vibroacoustic model of the periodic composite structure with porous lining can be established. The problem can be solved by adopting the preconditioning method by Hull [32] then. The periodically rib-stiffened model is discussed as an example. The novelty here is the combination of the Biot theory and SHS for the poroelastic problem with periodic boundary conditions.

In Section 2, detailed modeling procedures are given. The bonded-bonded case is given as an example and the solution procedures are illustrated. Then the validation and parameter analyses are provided in Section 3; Section 4 ends with the conclusion.

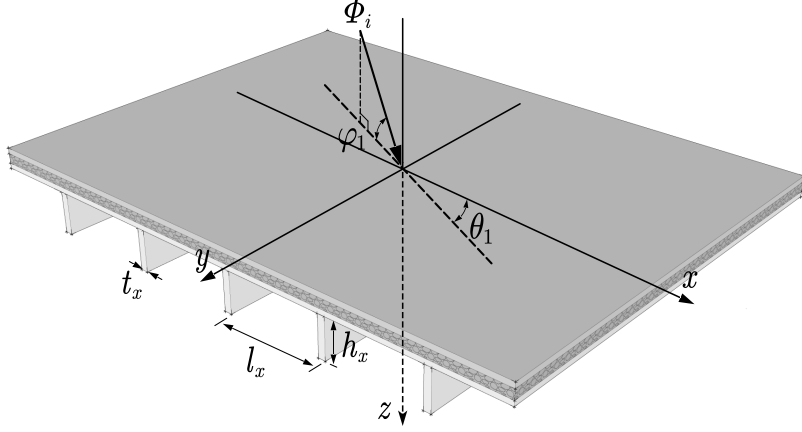


**Fig. 1.** A schematic diagram of the periodic composite model (ribs are exaggerated)

## 2. Modeling procedures for the periodic composite structure

The periodic composite structure is composed of a rib-stiffened double panel with porous lining, as shown in Fig.1; it is immersed in a stationary inviscid acoustic fluid. An incident wave  $\Phi_i = e^{j\omega t - j\mathbf{k}\mathbf{r}}$  transmits through the structure,  $\mathbf{k} = (k_x, k_y, k_z)$  is the incident wave vector,  $\mathbf{r} = (x, y, z)$ ,  $j = \sqrt{-1}$ . According to Fig.1,  $k_x = k_i \cos\varphi_1 \cos\theta_1$ ,  $k_y = k_i \cos\varphi_1 \sin\theta_1$ ,  $k_z = k_i \sin\varphi_1$ , here  $k_i$  is the incident wavenumber,  $\varphi_1$  and  $\theta_1$  are the incident elevation angle and azimuth angle respectively. The time dependent term  $e^{j\omega t}$  is omitted henceforth as the incident wave is time harmonic [7, 33]. The space occupied by acoustic fluid on both sides is assumed to be semi-infinite and lossless; the density and sound velocity are designated as  $\rho_i, c_i$  and  $\rho_t, c_t$  for the incident and transmitted side respectively.

The ribs are periodically placed along  $x$  at a spacing  $l_x$ , and extend infinitely along  $y$ ; the thickness and height are  $t_x, h_x$  (as shown in Fig.1). The longitudinal deformation of ribs is ignored as the  $y$  dimension is infinite.

### 2.1. The velocity potentials in acoustic media

As periodic cavities between the ribs are formed, the SHS is used [22] to express the velocity potential  $\Phi_1$  of the incident side

$$\Phi_1 = \Phi_i + \Phi_r = e^{-j\mathbf{k}\mathbf{r}} + \sum_m R_m e^{-j\mathbf{k}_i^m \mathbf{r}} \quad (1)$$

where  $\mathbf{k}_i^m = (k_{i,x}^m, k_{i,y}^m, k_{i,z}^m)$  is the wave vector;  $R_m$  is the unknown amplitude of reflected wave harmonics;  $k_{i,x}^m = k_x + 2m\pi/l_x$ ,  $k_{i,y}^m = k_y$ ; integer  $m \in [-\infty, \infty]$ . According to wave equation  $\partial^2 \Phi_1 / \partial t^2 = c_i^2 \nabla^2 \Phi_1$ ,  $k_i = \omega/c_i$ ,  $k_{i,z}^m = \sqrt{k_i^2 - (k_{i,x}^m)^2 - (k_{i,y}^m)^2}$ .

The velocity potential of transmitted side can be expressed as

$$\Phi_2 = \sum_m T_m e^{-j\mathbf{k}_t^m \mathbf{r}} \quad (2)$$

here  $\mathbf{k}_t^m = (k_{t,x}^m, k_{t,y}^m, k_{t,z}^m)$  is the wave vector;  $T_m$  is the unknown amplitude of transmitted wave harmonics; integer  $m \in [-\infty, \infty]$ . According to the law of refraction [34], the wave vector component  $k_{t,x}^m = k_{i,x}^m$ ,  $k_{t,y}^m = k_{i,y}^m$ ; substitute Eq.(2) in wave equation  $\partial^2 \Phi_2 / \partial t^2 = c_t^2 \nabla^2 \Phi_2$ , then  $k_{t,z}^m = \sqrt{k_t^2 - (k_{t,x}^m)^2 - (k_{t,y}^m)^2}$ ,  $k_t = \omega / c_t$ .

Once the velocity potential  $\Phi$  is determined, the corresponding sound pressure  $p$  and acoustic particle velocity  $\mathbf{v}$  can be obtained by  $p = \rho \frac{\partial \Phi}{\partial t}$ ,  $\mathbf{v} = -\nabla \Phi$ .

### 2.2. In-plane and transverse vibration of face panels

The two face panels are considered as isotropic thin plates. Their thickness, displacement along x, y and z are denoted as  $h_i, u_i, v_i, w_i$  respectively, here  $i = 1, 2$  correspond to the incident and transmitted side panel. When in-plane force and moment are present, the vibration equations are [35]

$$\mathcal{L}_i(u, v) = f_x, \quad \mathcal{L}_t(w) = f_z - \frac{\partial \mathcal{M}_x}{\partial y} + \frac{\partial \mathcal{M}_y}{\partial x} \quad (3)$$

where

$$\mathcal{L}_i(u, v) = \rho h \frac{\partial^2 u}{\partial t^2} - D_p \frac{\partial}{\partial x} \left( \frac{\partial u}{\partial x} + \nu \frac{\partial v}{\partial y} \right) - Gh \frac{\partial}{\partial y} \left( \frac{\partial u}{\partial y} + \frac{\partial v}{\partial x} \right) \quad (4)$$

$$\mathcal{L}_t(w) = D \nabla^4 w + \rho h \frac{\partial^2 w}{\partial t^2} \quad (5)$$

are the in-plane vibration and transverse vibration operator;  $f_z, f_x$  are the external forces along z and x; the in-plane moment  $\mathbf{m} = \mathcal{M}_x \mathbf{i}_x + \mathcal{M}_y \mathbf{i}_y$ ,  $\mathbf{i}_x$  and  $\mathbf{i}_y$  are unit vectors along x and y;  $\rho$  is the density,  $h$  is the thickness,  $D_p$  is the in-plane stiffness,  $G$  is the shear modulus, and  $D$  is the bending stiffness. The panel displacement  $\mathbf{u}_i = (u_i, v_i, w_i)$  is expressed as

$$\mathbf{u}_i = \sum_m \mathbf{U}_i^m e^{-j(k_x^m x + k_y^m y)} \quad (6)$$

here  $k_x^m = k_{i,x}^m$ ,  $k_y^m = k_{i,y}^m$  according to the law of refraction;  $\mathbf{U}_i^m = (U_i^m, V_i^m, W_i^m)$  is the unknown component amplitude vector; integer  $m \in [-\infty, \infty]$ .

### 2.3. Flexural vibration and rotation of ribs

The flexural vibration of ribs is modeled by the Bernoulli-Euler model and Timoshenko model here; a comparison between them is made. The rotation of ribs is modeled by the torsional wave equation.

The Bernoulli-Euler beam (BE-B) equation is [36]

$$EI \frac{\partial^4 w}{\partial y^4} + \rho A \frac{\partial^2 w}{\partial t^2} = f_z$$

where  $w$  is the displacement,  $\rho$  is the density,  $E$  is Young's modulus,  $I$  is the second moment of area,  $A$  is the cross-section area and  $f_z$  is the external force. The Timoshenko beam (TS-B) equation is [36]

$$EI \frac{\partial^4 w}{\partial y^4} - \rho I \left( 1 + \frac{E}{G\kappa} \right) \frac{\partial^4 w}{\partial y^2 \partial t^2} + \rho A \frac{\partial^2 w}{\partial t^2} + \frac{\rho^2 I}{G\kappa} \frac{\partial^4 w}{\partial t^4} = f_z - \frac{EI}{GA\kappa} \frac{\partial^2 f_z}{\partial y^2} + \frac{\rho I}{GA\kappa} \frac{\partial^2 f_z}{\partial t^2}$$

where  $G$  is the shear modulus,  $\kappa$  is the shear correction factor.

The rotation is determined by [37]

$$GI_p \frac{\partial^2 \theta_y}{\partial y^2} - \rho I_p \frac{\partial^2 \theta_y}{\partial t^2} = m_y$$

where  $I_p$  is the polar moment of inertia,  $m_y$  is the external moment;  $\theta_y = \partial w_2 / \partial x$  is the clockwise angle of rotation about the rib-panel interface, here  $w_2$  is the panel displacement.

Then the forces exerted on the transmitted side plate can be obtained using the above equations and the displacement continuity condition. The results are

$$f_z = K_z w_2, \quad m_y = K_y \sum_m j k_x^m W_2^m e^{-j(k_x^m x + k_y^m y)} \quad (7)$$

here  $K_y = GI_p k_y^2 - \rho I_p \omega^2$ , while

$$K_z = \begin{cases} EI k_y^4 - \rho A \omega^2, & \text{For BE-B case} \\ \frac{EI k_y^4 - \rho I (1 + E/G\kappa) k_y^2 \omega^2 - \rho A \omega^2 + (\rho^2 I/G\kappa) \omega^4}{1 + (EI/GA\kappa) k_y^2 - (\rho I/GA\kappa) \omega^2}, & \text{For TS-B case} \end{cases} \quad (8)$$

depending on the beam model.

The resultant force exerted by the periodic ribs can then be written as

$$F_z = \sum_n f_z \delta(x - nl_x) + \sum_n \frac{\partial m_y}{\partial x} \delta(x - nl_x) \quad (9)$$

here  $n \in [-\infty, \infty]$ . It becomes

$$F_z = \frac{1}{l_x} \sum_n \sum_m [K_z W_2^m + (k_x^m)^2 K_y W_2^m] e^{-j(k_x^m x + k_y^m y)} e^{j2\pi n x / l_x} \quad (10)$$

utilizing Eq.(7) and the Poisson summation formula [33]

$$\sum_{n=-\infty, \infty} \delta(x - nl_x) = \frac{1}{l_x} \sum_{n=-\infty, \infty} e^{j2\pi n x / l_x} \quad (11)$$

A double summation is present, which makes the problem complicated and cumbersome. An index separation identity is utilized to eliminate it.

#### 2.4. The poroelastic field with periodic boundary conditions

In poroelastic problems, appropriate porous modeling procedure is quite absent when the periodic boundary conditions are present. An extended and generalized method for porous modeling is given, compared to the previous ones [15, 18]. The wave components in the porous media are expressed as six groups of harmonics here, according to their propagation wavenumbers; then the poroelastic field with periodic boundary conditions is obtained. The porous material is assumed to be isotropic with homogeneous cylindrical pores to get a neat formulation.

The poroelastic equations expressed by solid and fluid displacement  $\mathbf{u}^s, \mathbf{u}^f$  are [38, 15]

$$-\omega^2 (\rho_{11}^* \mathbf{u}^s + \rho_{12}^* \mathbf{u}^f) = (A + N) \nabla \nabla \cdot \mathbf{u}^s + N \nabla^2 \mathbf{u}^s + Q \nabla \nabla \cdot \mathbf{u}^f \quad (12)$$

$$-\omega^2 (\rho_{22}^* \mathbf{u}^f + \rho_{12}^* \mathbf{u}^s) = R \nabla \nabla \cdot \mathbf{u}^f + Q \nabla \nabla \cdot \mathbf{u}^s \quad (13)$$

where  $\rho_{11}^* = \rho_{11} + b/j\omega$ ,  $\rho_{12}^* = \rho_{12} - b/j\omega$ ,  $\rho_{22}^* = \rho_{22} + b/j\omega$ ,  $\rho_{11} = \rho_1 + \rho_a$ ,  $\rho_{12} = -\rho_a = \rho_2(1 - \epsilon')$ ,  $\rho_{22} = \rho_2 + \rho_a$ ,  $b = j\omega\epsilon'\rho_2(\rho_c^*/\rho_f - 1)$ ,  $\rho_c^* = \rho_f[1 - 2T_c(\lambda_1)/\lambda_1]^{-1}$ ,  $\lambda_1 = \lambda_c\sqrt{-j}$ ,  $\lambda_c = \sqrt{8\omega\rho_f\epsilon'/\phi\sigma}$ ;  $\rho_f$  is the density of ambient fluid;  $\phi$  is the porosity;  $\rho_1$  and  $\rho_2 = \phi\rho_f$  are the bulk solid and fluid densities;  $\epsilon'$  is the geometrical structure factor;  $\sigma$  is the flow resistivity; auxiliary function  $T_c(x) = J_1(x)/J_0(x)$ ,  $J_1(x)$  and  $J_0(x)$  are the Bessel functions of the first kind, first and zero order respectively. Parameter  $A = \nu_s E_s / (1 + \nu_s)(1 - 2\nu_s)$  is the first Lamé constant;  $N = E_s / 2(1 + \nu_s)$  is the shear modulus; the two coupling parameter  $Q = (1 - \phi)E_f$ ,  $R = \phi E_f$ , here  $E_f = \rho_f c_f^2 [1 + 2(\gamma - 1)T_c(\lambda_2)/\lambda_2]^{-1}$  is the bulk modulus of fluid in the pores;  $c_f$  is the sound velocity of fluid in pores;  $\gamma$  is the ratio of specific heats; auxiliary variable  $\lambda_2 = \lambda_c\sqrt{-j}N_{Pr}$ ,  $N_{Pr}$  is the Prandtl number in pores.

The poroelastic equations Eqs.(12)-(13) can be reduced to two wave equations [15, 18] (a fourth order equation and a second order equation) when two scalar potentials  $\varphi^s = \nabla \cdot \mathbf{u}^s$ ,  $\varphi^f = \nabla \cdot \mathbf{u}^f$  and two vector potentials  $\Psi^s = \nabla \times \mathbf{u}^s$ ,  $\Psi^f = \nabla \times \mathbf{u}^f$  are introduced; these potentials are the dilatational and rotational strains of corresponding phase [38, 15]. The wavenumbers correspond to the wave equations are

$$\{k_1^2, k_2^2\} = A_1/2 \pm \sqrt{A_1^2/4 - A_2}, \quad k_3^2 = \omega^2/N(\rho_{11}^* - \rho_{12}^*\rho_{12}^*/\rho_{22}^*) \quad (14)$$

here the auxiliary term  $A_1 = \omega^2(\rho_{11}^*R - 2\rho_{12}^*Q + \rho_{22}^*P)/(PR - Q^2)$ ,  $A_2 = \omega^4(\rho_{11}^*\rho_{22}^* - \rho_{12}^*\rho_{12}^*)/(PR - Q^2)$ ,  $P = A + 2N$ .

Utilizing SHS, the amplitude of solid phase strain  $e^s = \varphi^s$ ,  $\Omega^s = \Psi^s$  are written as

$$|e^s| = \sum_m e^{-j(k_x^m x + k_y^m y)} \left( C_1^m e^{-jk_{1,z}^m z} + C_2^m e^{jk_{1,z}^m z} + C_3^m e^{-jk_{2,z}^m z} + C_4^m e^{jk_{2,z}^m z} \right) \quad (15)$$

$$|\Omega^s| = \sum_m e^{-j(k_x^m x + k_y^m y)} \left( C_5^m e^{-jk_{3,z}^m z} + C_6^m e^{jk_{3,z}^m z} \right) \quad (16)$$

here  $C_i^m$  ( $i = 1, 2, \dots, 6$ ) are the unknown amplitude of harmonic components;  $k_{1,z}^m, k_{2,z}^m, k_{3,z}^m$  are the z component of the corresponding wave vectors; the law of refraction is used here. According to Eqs.(12)-(13), the amplitude of fluid phase strain  $e^f = \varphi^f$ ,  $\Omega^f = \Psi^f$  are

$$|e^f| = \sum_m e^{-j(k_x^m x + k_y^m y)} \left( b_1^m e^{-jk_{1,z}^m z} + b_2^m e^{jk_{1,z}^m z} + b_3^m e^{-jk_{2,z}^m z} + b_4^m e^{jk_{2,z}^m z} \right) \quad (17)$$

$$|\Omega^f| = g\epsilon^s \quad (18)$$

here  $b_1^m = (a_1 - a_2 k_1^2)C_1^m$ ,  $b_2^m = (a_1 - a_2 k_1^2)C_2^m$ ,  $b_3^m = (a_1 - a_2 k_2^2)C_3^m$ ,  $b_4^m = (a_1 - a_2 k_2^2)C_4^m$ ,  $g = -\rho_{12}^*/\rho_{22}^*$ ; the auxiliary term  $a_1 = (\rho_{11}^*R - \rho_{12}^*Q)/(\rho_{22}^*Q - \rho_{12}^*R)$ ,  $a_2 = (PR - Q^2)/\omega^2(\rho_{22}^*Q - \rho_{12}^*R)$ . Using the definition of potentials and substituting Eqs.(15)-(18) into Eqs.(12)-(13), then  $k_{i,z}^m = \sqrt{k_i^2 - (k_x^m)^2 - (k_y^m)^2}$  ( $i=1,2,3$ ) can be obtained.

It is assumed that the field variables are composed of six groups of harmonics (i.e.  $\pm k_{1,z}^m, \pm k_{2,z}^m, \pm k_{3,z}^m$ ) here, while only six wave components are included in previous papers [8, 15]. According to the definition of potentials, the displacement  $\mathbf{u} = [u_x^s, u_y^s, u_z^s, u_x^f, u_y^f, u_z^f]^T$  can be deduced using a similar procedure as Bolton [15] with  $\nabla \cdot \boldsymbol{\Omega}^s = 0$  and  $\nabla \cdot \boldsymbol{\Omega}^f = 0$  [39]

$$\mathbf{u} = \sum_m e^{-j(k_x^m x + k_y^m y)} \mathbf{Y}_m \mathbf{e}_m \mathbf{C}_m \quad (19)$$

where

$$\mathbf{e}_m = \text{diag}(e^{-jk_{1,z}^m z}, e^{jk_{1,z}^m z}, e^{-jk_{2,z}^m z}, e^{jk_{2,z}^m z}, e^{-jk_{3,z}^m z}, e^{jk_{3,z}^m z}) \quad (20)$$

$$\mathbf{C}_m = [C_1^m, C_2^m, C_3^m, C_4^m, C_5^m, C_6^m]^T \quad (21)$$

matrix  $\mathbf{e}_m$  is a  $6 \times 6$  diagonal matrix. The elements of coefficient matrix  $\mathbf{Y}_m$  are given in Appendix A. The forces in porous media are [8, 38]

$$\sigma_{ij} = 2N e_{ij} + (Ae^s + Qe^f) \delta_{ij} \quad (22)$$

$$s = Qe^s + Re^f \quad (23)$$

where  $\sigma_{ij}$  and  $s$  are the forces in solid and fluid phase;  $e_{ij}$  is the normal strain ( $i = j$ ) or shear strain ( $i \neq j$ );  $\delta_{ij}$  is the Kronecker delta

$$e_{ij} = \begin{cases} \partial u_i / \partial x_i, & i = j \\ \frac{1}{2} (\partial u_i / \partial x_j + \partial u_j / \partial x_i), & i \neq j \end{cases}, \quad \delta_{ij} = \begin{cases} 1, & i = j \\ 0, & i \neq j \end{cases} \quad (24)$$

### 2.5. Boundary conditions

The boundary condition notation of Bolton [15] is used; the connection type can be bonded-bonded (BB), bonded-unbonded (BU) and unbonded-unbonded (UU). The related boundary conditions are not given here, as they can be found in Bolton [15], Zhou [18] and Liu [19] etc. Note that a right-handed coordinate system is used here, while Bolton and Zhou used the left-handed one, Liu used a right-handed one. The detailed expressions are identical for the 2D case, but in the 3D case, some modifications should be made between the two coordinate systems.

## 2.6. System equations and solution procedures

The bonded-bonded case is used as an example to demonstrate the solution procedure. Related boundary conditions are

$$\begin{aligned}
& \text{(i)} \quad -j\omega \frac{\partial \Phi_1}{\partial z} = \frac{\partial^2 w_1}{\partial t^2} \quad \text{(ii)} \quad \mathcal{L}_i(u_1, v_1) = \tau_{zx} \\
& \text{(iii)} \quad \mathcal{L}_t(w_1) = j\omega \rho_i \Phi_1 + (\sigma_z + s) - \frac{h_1}{2} \left( \frac{\partial \tau_{zx}}{\partial x} + \frac{\partial \tau_{zy}}{\partial y} \right) \\
& \text{(iv)} \quad u_z^s = w_1 \quad \text{(v)} \quad u_z^f = w_1 \quad \text{(vi)} \quad u_x^s = u_1 - \frac{h_1}{2} \frac{\partial w_1}{\partial x} \\
& \text{(vii)} \quad u_y^s = v_1 - \frac{h_1}{2} \frac{\partial w_1}{\partial y} \quad \text{(viii)} \quad u_z^s = w_2 \quad \text{(ix)} \quad u_z^f = w_2 \\
& \text{(x)} \quad u_x^s = u_2 + \frac{h_2}{2} \frac{\partial w_2}{\partial x} \quad \text{(xi)} \quad u_y^s = v_2 + \frac{h_2}{2} \frac{\partial w_2}{\partial y} \\
& \text{(xii)} \quad \mathcal{L}_i(u_2, v_2) = -\tau_{zx} \\
& \text{(xiii)} \quad \mathcal{L}_t(w_2) = -j\omega \rho_t \Phi_2 - (\sigma_z + s) - \frac{h_2}{2} \left( \frac{\partial \tau_{zx}}{\partial x} + \frac{\partial \tau_{zy}}{\partial y} \right) - F_z \\
& \text{(xiv)} \quad -j\omega \frac{\partial \Phi_2}{\partial z} = \frac{\partial^2 w_2}{\partial t^2} \tag{25}
\end{aligned}$$

where  $F_z$  is the resultant force exerted by the ribs in Eq.(10); (i)-(xiv) are applied on the domain interfaces or panel middle surfaces [15, 18].

To eliminate the summation index used, the orthogonal property below

$$\int_{-l_x/2}^{l_x/2} e^{-j(k_x^m x + k_y^m y)} e^{j(k_x^p x + k_y^p y)} dx = \begin{cases} l_x, & m = p \\ 0, & m \neq p \end{cases} \tag{26}$$

and a double summation identity analogous to Hull [32]

$$\sum_{n=-\infty}^{+\infty} \sum_{m=-\infty}^{+\infty} W_m e^{-jk_x^m x} e^{j2\pi n x / l_x} = \sum_{n=-\infty}^{+\infty} W_n \sum_{m=-\infty}^{+\infty} e^{-jk_x^m x} \tag{27}$$

are used. The derivation of Eq.(27) is given in Appendix B.

Substitute Eqs.(1), (2), (6), (10), (19), (22) and (23) into (25), and utilize Eqs.(26)-(27), Eq.(25) becomes

$$\mathbf{A}_m \mathbf{x}_m = \sum_n \mathbf{B}_n \mathbf{x}_n + \begin{cases} \mathbf{p}, & m = 0 \\ \mathbf{0}, & m \neq 0 \end{cases} \tag{28}$$

where

$$\mathbf{x}_m = [C_1^m, C_2^m, C_3^m, C_4^m, C_5^m, C_6^m, U_1^m, V_1^m, W_1^m, U_2^m, V_2^m, W_2^m, R_m, T_m]^T$$

here  $\mathbf{0}$  is a zero  $14 \times 1$  vector; all the elements of corresponding matrices and vector in Eq.(28) are given in Appendix C. Eq.(28) should be solved for every integer  $m, n \in [-\infty, +\infty]$ , thus is a matrix system of infinite dimension.



### 3. Results and discussions

This part begins with overview of the convergence characteristics; then the validation is conducted; at last, several parameter analyses are performed. The ribs of rectangular cross-section and the porous parameters given in [15, 18, 19] are utilized. The detailed values are listed in Table 1; they are used if no other values are specified hereinafter. The random STL is calculated in 1/24 octave bands using the 2D Simpson's rule;  $\varphi_{\min} = \pi/10$  [15] as no convective flow is present; the integration domain of  $\varphi_1$  and  $\theta_1$  are split up into 36 and 90 subdivisions respectively.

**Table 1**

Parameters in the periodic composite structure: air gap thickness  $h_a=14\text{mm}$  for BU case;  $h_{a1}=2\text{mm}$ ,  $h_{a2}=6\text{mm}$  for incident and transmitted side in UU case; characteristic thickness  $d = h_p, (h_p + h_a)$  and  $(h_p + h_{a1} + h_{a2})$  for the BB, BU and UU case respectively; the gap properties  $\rho_g = \rho_i, c_g = c_i$  and transmitted side media properties  $\rho_t = \rho_i, c_t = c_i$  here

Parameters	Physical description	Value
Acoustic media		
$\rho_i$	density of incident side media	1.205 kg/m <sup>3</sup>
$c_i$	sound velocity of incident side media	343 m/s
Double-panels		
$\rho_p$	density of face panels	2700 kg/m <sup>3</sup>
$E_p$	Young's modulus of face panels	$70 \times 10^9 \text{Pa}$
$\nu_p$	Poisson's ratio of face panels	0.33
$h_1$	face panel thickness of incident side	1.27 mm
$h_2$	face panel thickness of transmitted side	0.762 mm
$h_p$	thickness of porous core	27 mm
Ribs		
$l_x$	rib spacing along x	$50d$
$t_x$	rib thickness	1 mm
$h_x$	rib height	20 mm
Porous media		
$\rho_s$	density of solid phase	30 kg/m <sup>3</sup>
$\rho_f$	density of fluid phase	1.205 kg/m <sup>3</sup>
$E_s$	Young's modulus of solid phase	$8 \times 10^5 \text{Pa}$
$\nu_s$	Poisson's ratio of solid phase	0.4
$\eta_s$	loss factor of solid phase	0.265
$\phi$	the porosity	0.9
$\epsilon'$	geometrical structure factor	7.8
$\sigma$	flow resistance	$2.5 \times 10^4 \text{ MKS Rayls/m}$

#### 3.1. Overview of the convergence characteristics

A truncation procedure is needed to solve the infinite matrix equation Eq.(33). The convergence criteria is taken as  $\Delta\text{STL} = 0.1\text{dB}$  under the maximum computation frequency ( $f=10\text{kHz}$ ); that is, when the change in STL by one additional  $\hat{m}$  item is less than  $\Delta\text{STL}$ , it is considered as converged. A typical convergence curve of the three boundary

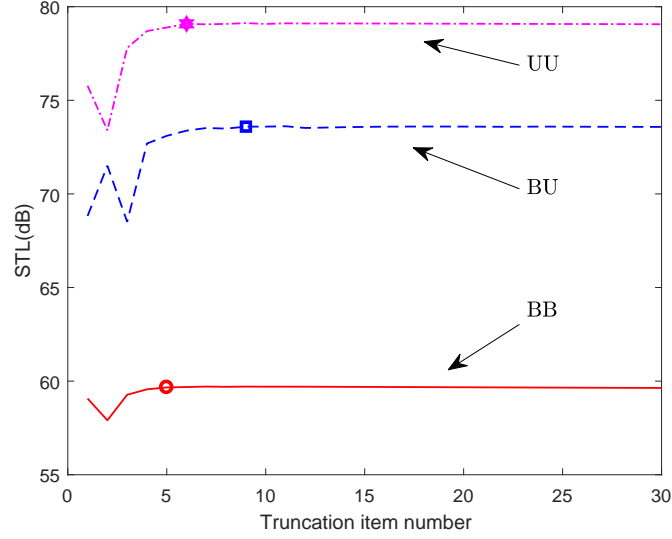


**Fig. 2.** Variation of STL with the truncation item number  $\hat{m}$  at  $f=10\text{kHz}$  ( $l_x=50d$ )

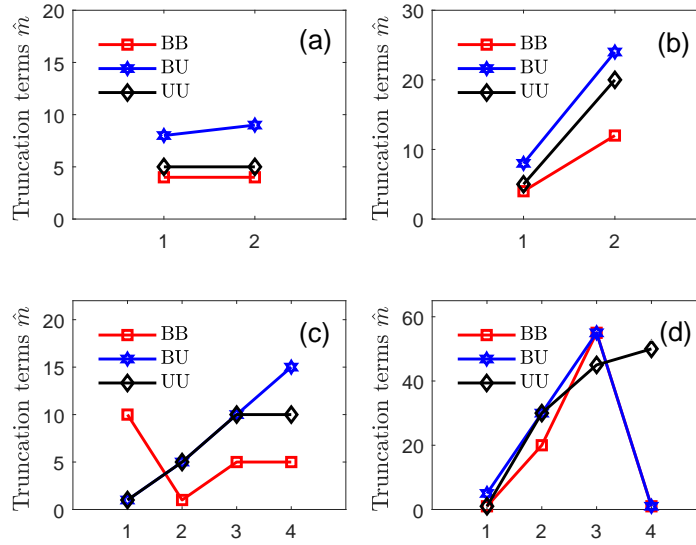


**Fig. 3.** Truncation item number  $\hat{m}$  needed for (a) Beam model (1 BE-B, 2 TS-B); (b) Torsion motion (1-with, 2-w/o); (c) Rib spacing  $l_x$  case; (d) Area moment of inertia  $I$  case

conditions is given in Fig.2. Different marks (circles, squares and hexagrams for BB, BU and UU cases respectively) here show the convergence points in the given figure.

The truncation item number  $\hat{m}$  needed for different parameter cases are shown in Fig.3. It can be seen that  $\hat{m}$  is dependent on the boundary conditions and parameter values. A related study concerning  $\hat{m}$  is in progress, however, no conclusion can be drawn for now.

As a result, one needs to determine  $\hat{m}$  in every numerical case when the method proposed here is used. This is the main drawback of the proposed method here.

### 3.2. Model Validation

The poroelastic field representation is validated using theoretical results of unribbed double panel structure with porous lining by Bolton [15] (2D), Zhou [18] (3D) and Liu [19] (3D). The unribbed case corresponds to  $\mathbf{B}$  is a zero matrix and  $l_x$  tends to infinity here. The rib-stiffened configurations here are validated with FEM results, as no theoretical or experimental result can be found in the open literature so far, to the author's knowledge.

#### 3.2.1. Validation of poroelastic field representation

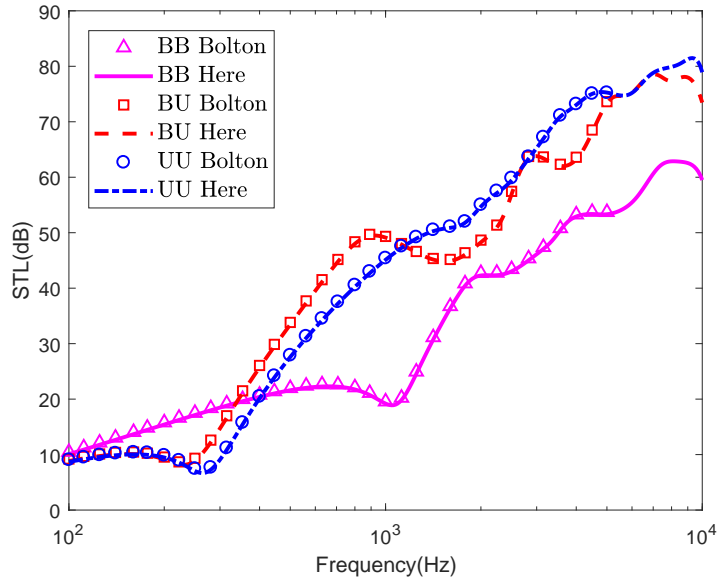
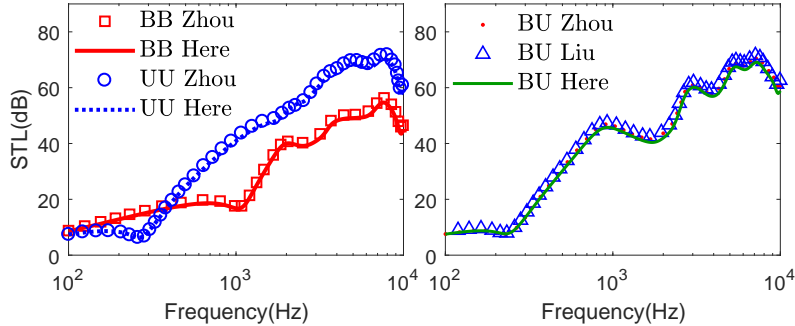


Fig. 4. Porous modeling validation with Bolton

The model is first downgraded to 2D by setting  $\theta_1=0$ . Result comparisons with Bolton are presented in Fig.4 and the consistency is good. Then validation with Zhou [18] and Liu [19] when external flow Mach number  $M = 0$  is performed. The results are shown in Fig.5. The correctness of the poroelastic field representation is confirmed by these two cases.

#### 3.2.2. Oblique incident STL validation with FEM results

Several oblique incident cases are compared, as the random STL is clearly related to the oblique incident case according to Eq.(35). The oblique incident STL are used in Figs.7-9 for the vertical axis values.



**Fig. 5.** Porous modeling validation with Zhou and Liu

The FEM models are formed by the mixed displacement-pressure form Biot-Allard equations [38]; the viscous and thermal characteristic length required are obtained using an equivalent relationship [9, 38]  $\Lambda = (8\mu_f\epsilon'/\sigma\phi)^{1/2}$ ,  $\Lambda' = 2\Lambda$ , here  $\mu_f$  is the dynamic viscosity of fluid in pores. Perfectly matched layer (PML) and periodic boundary conditions (periodic BC) are used. Symmetric boundary conditions (symmetric BC) for y coordinate are used, as the structure is infinite in the y direction. A schematic description of the FEM configuration is shown in Fig.6. The FEM calculations are performed using COMSOL.

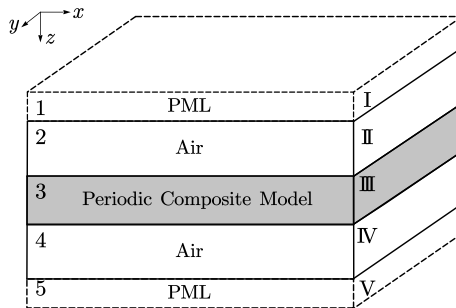


**Fig. 6.** Schematic diagram of the FEM model: periodic BC is applied on the surfaces vertical to x (surface I-V etc.); symmetric BC is applied on the surfaces vertical to y (surface 1-5 etc.)

The results are given in Figs.7-9 for the BB, BU and UU case respectively. They are in good overall coherence with FEM results, while critical local differences are satisfactory. For all oblique incidence cases, the STL differences are less than 2dB (absolute value) on average; in the meantime, the relative differences are all no more than 10% of the FEM results on average, despite few extrema occur asynchronously. This is another evidence of the usability of the proposed method here.

Time used in the 3D oblique incidence calculations are listed in Table 2. The efficiency is pronounced, while the FEM is expensive due to refined model required by large size change. However, the drawback should be noted, as the convergence check can take up to 69.76%, 73.34% and 75.45% of the total calculation time on average. For the 3D random

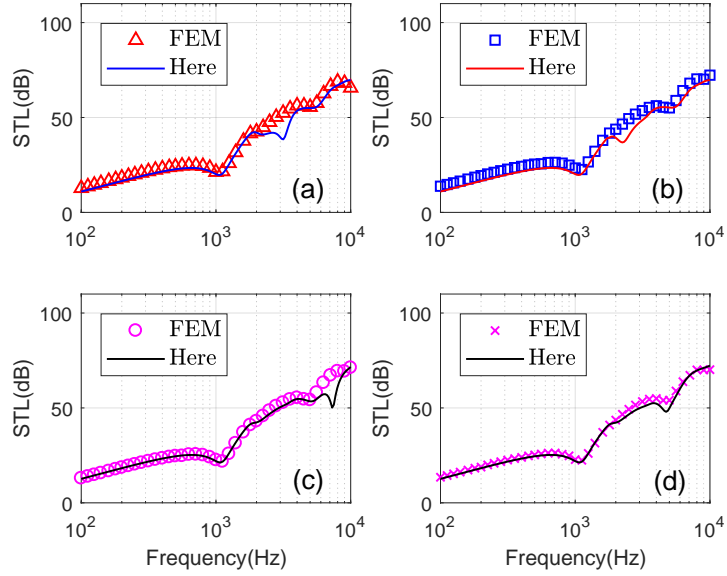


**Fig. 7.** Validation of the 3D oblique incidence BB boundary case: (a)  $\varphi_1 = \pi/4, \theta_1 = \pi/4$ ; (b)  $\varphi_1 = \pi/4, \theta_1 = \pi/3$ ; (c)  $\varphi_1 = \pi/3, \theta_1 = \pi/4$ ; (d)  $\varphi_1 = \pi/3, \theta_1 = \pi/3$

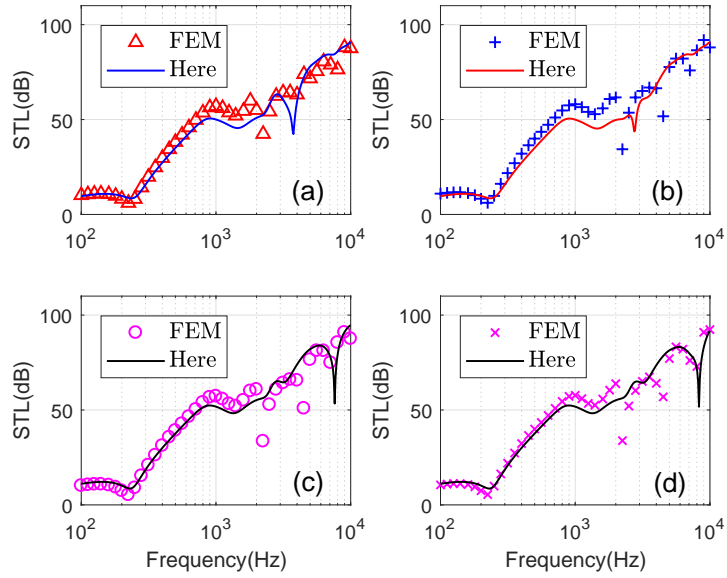


**Fig. 8.** Validation of the 3D oblique incidence BU boundary case: (a)  $\varphi_1 = \pi/4, \theta_1 = \pi/4$ ; (b)  $\varphi_1 = \pi/4, \theta_1 = \pi/3$ ; (c)  $\varphi_1 = \pi/3, \theta_1 = \pi/4$ ; (d)  $\varphi_1 = \pi/3, \theta_1 = \pi/3$

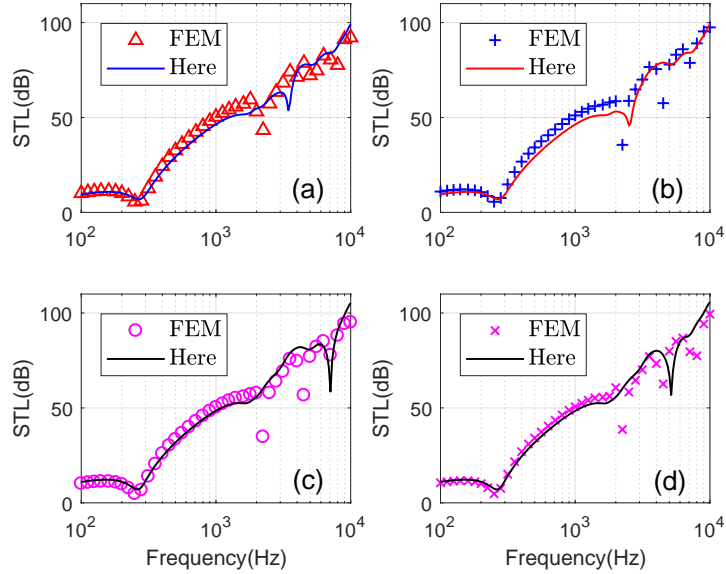


**Fig. 9.** Validation of the 3D oblique incidence UU boundary case: (a)  $\varphi_1 = \pi/4$ ,  $\theta_1 = \pi/4$ ; (b)  $\varphi_1 = \pi/4$ ,  $\theta_1 = \pi/3$ ; (c)  $\varphi_1 = \pi/3$ ,  $\theta_1 = \pi/4$ ; (d)  $\varphi_1 = \pi/3$ ,  $\theta_1 = \pi/3$

incidence, more than 80% of the total calculation time can be used; thus an improvement is needed. A related study is in progress.

**Table 2**

Total time used for the oblique incidence cases: a periodic span along x is used in the FE Model; the unstructured 3D elements are 310228, 202882 and 270319 for BB, BU and UU

Angle ( $\varphi_1, \theta_1$ )	BB		BU		UU	
	FEM (s)	Here (s)	FEM (s)	Here (s)	FEM (s)	Here (s)
$(\pi/4, \pi/4)$	39482	6.655	14132	6.206	10593	5.255
$(\pi/4, \pi/3)$	65396	4.859	13690	5.538	10461	4.261
$(\pi/3, \pi/4)$	53677	5.262	13940	6.482	10638	5.136
$(\pi/3, \pi/3)$	40299	5.524	15151	6.557	10823	5.606

### 3.3. Influence of rib reinforcement model on the STL

The beam models mentioned above are used. The STL and its difference defined as the Timoshenko beam case minus the Bernoulli-Euler beam case for different boundary conditions are shown in Fig.10.

An overall consistency is found for the BB case, while 2dB or so differences (under most frequencies) are found for the BU and UU case. It is confirmed by FEM that combined flexural and torsional modes of ribs around 1372Hz appeared, one of these modes is shown in Fig.11 (UU case eigenfrequency 1375Hz). The FEM configuration of section 3.2.2 is used hereinafter. Due to the consistency of the two beam models, the Bernoulli-Euler beam model is more preferable. It is used in the following.

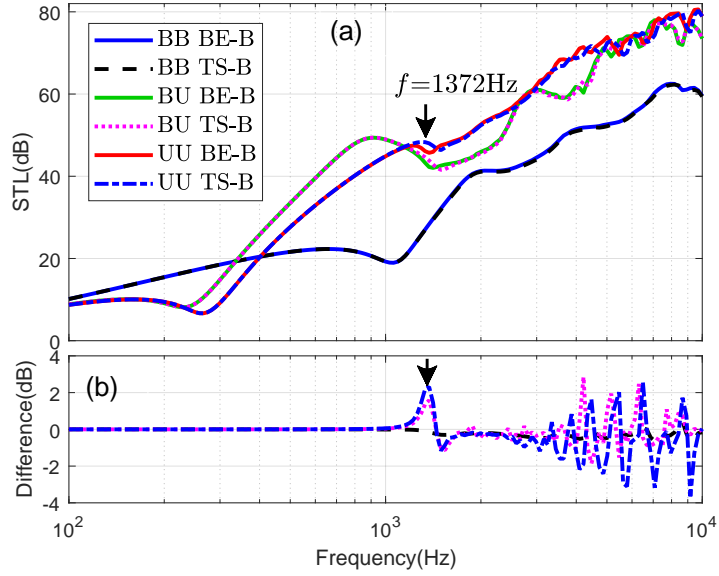


**Fig. 10.** Results of different beam models (a) the STL of different cases; (b) the difference between beam models in each boundary condition. The legends of (b) are the same as (a)

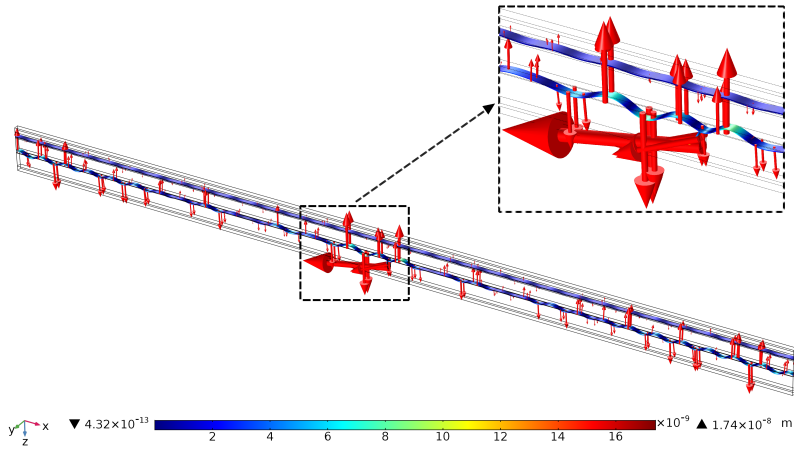


**Fig. 11.** UU case eigenfrequency 1375Hz. surface contour: the magnitude of total displacement; arrow: the magnitude and direction of displacement vector ; dotted line: the mode shape around ribs

### 3.4. Influence of torsional motion on the STL

The influence of torsion is discussed, though the transverse motion is more concerned in acoustics; detailed results are shown in Fig.12. The STL decrease emerges and can be larger than 5dB when the frequency exceeds 1454Hz (indicated in Fig.12). It is due to the emergence of the torsional mode of ribs (confirmed by FEM as shown in Fig.13). The STL

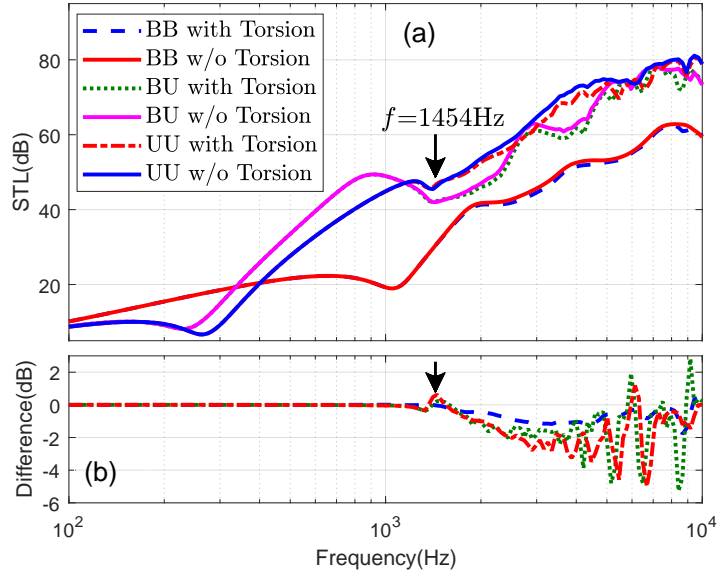


**Fig. 12.** Results of torsion motion (a) the STL when torsion is present or not; (b) the STL decrease when torsion is considered. The legends of (b) are the same as (a)

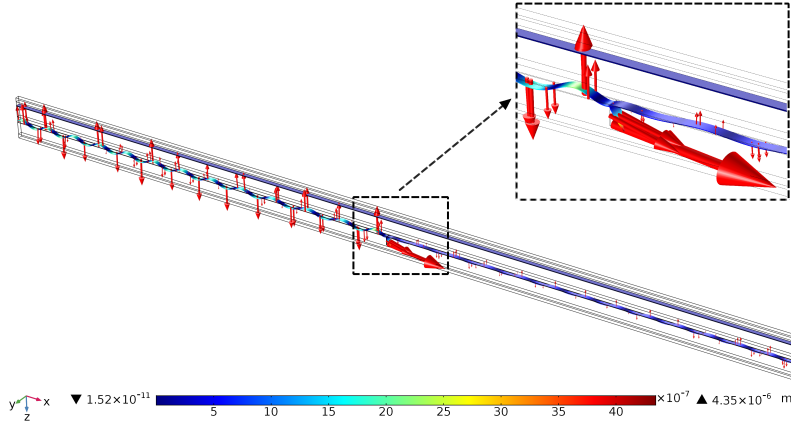


**Fig. 13.** BU case eigenfrequency 1455Hz: the torsional modes of ribs. surface contour: the magnitude of total displacement; arrow: the magnitude and direction of displacement vector ; dotted line: the mode shape around ribs

increases temporarily around the eigenfrequency, due to energy consumed by the torsional mode; then the torsion deteriorates the STL when apart from the eigenfrequency. Thus the torsion should be considered for its correlativity with the STL.

### 3.5. Influence of rib spacing on the STL

The results when  $l_x$  varies among  $l_x/d = 20, 50, 150$  versus the unribbed case are discussed. As the results of BB case are analogous to BU and UU case, the details are given in the supplementary materials to be brief.

In all the three cases, the STL is positively related to  $l_x$  in general; while a degradation occurs compared to the unribbed one. The overall trends are analogous to previous unribbed results [15, 18, 19]. As  $l_x$  decreases, more fluctuations emerge and the trough frequencies shift to lower ones (indicated in Figs.14-15). In fact, to avoid wave interference between ribs,  $l_x$  should be far greater than the coincidence wavelength  $\lambda_p$  of the face panels, which is [36]

$$\lambda_p = c_0/f_c, f_c = c_0^2/2\pi\sqrt{\rho_p h_i/D} \quad (36)$$

here  $c_0$  is the sound velocity of adjacent medium;  $i = 1, 2$  for the incident and transmitted side panel and  $\lambda_p = 36, 22$  (mm) respectively. When  $l_x$  is not large enough, the interference can be complex and fluctuations emerge.

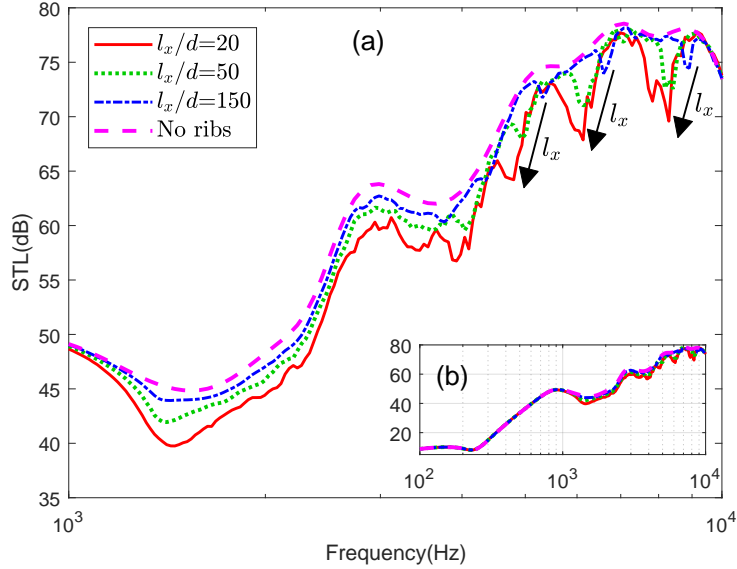


**Fig. 14.** Influence of  $l_x$  for the BU case : (a) STL at [1kHz,10kHz]; (b) overall STL trend. The black arrow indicates the direction  $l_x$  increases

In general, the STL is positively related to  $l_x$ , while the presence of ribs lower it, though direct transfer path is absent. This is due to the increase in flexural wave speed of the composite structure, i.e. the influence of stiffness increase is stronger than that of the mass increase [40] when ribs are present. To obtain better sound insulation performance, the ribs should be removed; at least,  $l_x$  should be increased, as  $l_x$  is related to the fluctuations and trough frequencies. Further investigations on the dispersion relation are needed to draw a quantitative conclusion.

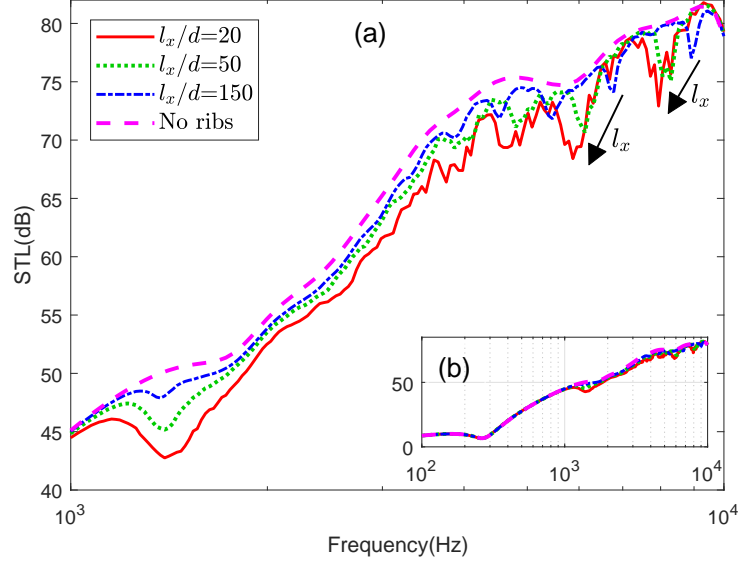


**Fig. 15.** Influence of  $l_x$  for the UU case : (a) STL at [1kHz,10kHz]; (b) overall STL trend. The black arrow indicates the direction  $l_x$  increases

### 3.6. Influence of area moment of inertia on the STL

To exclude the influence of mass change, the cross-section area of ribs  $A = t_x h_x$  is kept constant in this parameter case; for rectangular ribs, the area moment of inertia  $I$  is inversely proportional to  $t_x/h_x$  then. Thus the investigation is performed at  $t_x/h_x = 1/3, 1/5, 1/10, 1/20$ .

For the BB case, the influence of  $I$  is weak and the STL characteristics of unribbed structure dominate, as the structural connections are strong. The results are given in the supplementary materials. As shown in Figs.16-17, the STL decreases with the increase of  $I$  (as  $t_x/h_x$  decreases) under relatively low frequency range (i.e. between 100Hz and 1kHz); it's due to the increase of the phase velocity  $v_b$  of ribs [36]

$$v_b = (EI\omega^2/\rho A)^{1/4} \quad (37)$$

which is proportional to the group velocity here; thus better energy transmission and lower insulation as anticipated. In higher frequency range, the STL curve is analogous to the unribbed case [15, 18]; it is the superposition of unribbed STL and the fluctuations caused by ribs.

In general, the influence of  $I$  occurs in the low-frequency range; within this range,  $I$  is negatively related to the STL. To obtain better sound insulation in the low-frequency range, smaller area moment of inertia is preferred for similar structures.

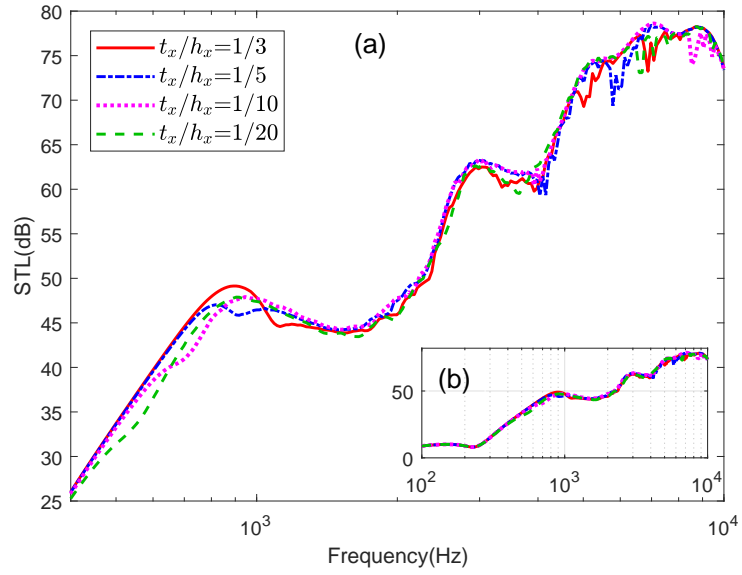


**Fig. 16.** Influence of  $I$  for BU case : (a) STL at [400Hz,10kHz]; (b) overall STL trend

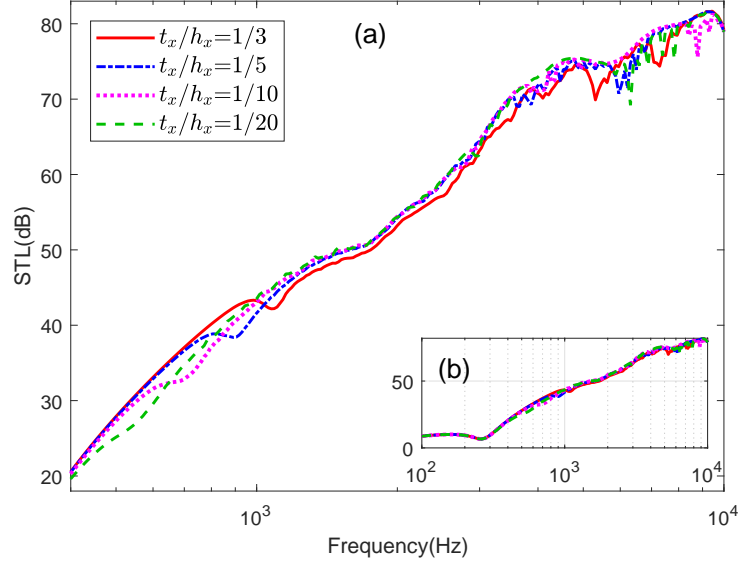


**Fig. 17.** Influence of  $I$  for UU case : (a) STL at [400Hz,10kHz]; (b) overall STL trend

#### 4. Conclusions

This paper develops a modeling procedure for the one-dimensional periodic composite structure with porous lining. The periodically rib-stiffened case is discussed utilizing the proposed method. The influence of the modeling parameters is studied, such as beam models, torsional motion, rib spacing and area moment of inertia.

It is found that the Bernoulli-Euler beam is enough to model the overall frequency response of ribs here. The torsion should not be ignored for its correlativity with the STL. In general, the STL is positively related to the rib spacing, while the use of ribs lowers it; smaller rib spacing means more STL fluctuations and worse sound insulation performance. The influence of area moment of inertia is mainly in the low-frequency range; it is negatively related to the STL there. The periodic ribs make the STL performance complicated, with fluctuations and decrease.

Despite the cumbersome truncation, the modeling procedure here for periodic poroelastic problems is efficient with considerable accuracy. As a feasible tool for combined periodic structure (metamaterial) and poroelastic problems, it can be promising in broadband sound modulation.

#### Acknowledgements

This work is supported by the National Natural Science Foundation of China (NSFC) No.11572137. The authors wish to thank some anonymous researchers and reviewers for their warm-hearted suggestions and comments.

## Appendix A. Elements of porous field variable coefficient matrix

To be brief, here  $k_x^m$ ,  $k_y^m$ ,  $k_{1,z}^m$ ,  $k_{2,z}^m$  and  $k_{3,z}^m$  are replaced by  $\alpha_m$ ,  $\beta$ ,  $\gamma_{1,m}$ ,  $\gamma_{2,m}$  and  $\gamma_{3,m}$  respectively, the elements of coefficient matrix  $\mathbf{Y}_m$  are

$$\begin{aligned}
Y_m(1,1) &= Y_m(1,2) = \frac{j\alpha_m}{k_1^2}, \quad Y_m(1,3) = Y_m(1,4) = \frac{j\alpha_m}{k_2^2} \\
Y_m(1,5) &= -\frac{j}{k_3^2\gamma_{3,m}}[(\gamma_{3,m}^2 + \beta^2)\cos\theta - \alpha_m\beta\sin\theta], \quad Y_m(1,6) = -Y_m(1,5) \\
Y_m(2,1) &= Y_m(2,2) = \frac{j\beta}{k_1^2}, \quad Y_m(2,3) = Y_m(2,4) = \frac{j\beta}{k_2^2} \\
Y_m(2,5) &= -\frac{j}{k_3^2\gamma_{3,m}}[(\gamma_{3,m}^2 + \alpha_m^2)\sin\theta - \alpha_m\beta\cos\theta], \quad Y_m(2,6) = -Y_m(2,5) \\
Y_m(3,1) &= \frac{j\gamma_{1,m}}{k_1^2}, \quad Y_m(3,2) = -Y_m(3,1) \\
Y_m(3,3) &= \frac{j\gamma_{2,m}}{k_2^2}, \quad Y_m(3,4) = -Y_m(3,3) \\
Y_m(3,5) &= \frac{j}{k_3^2}(\alpha_m\cos\theta + \beta\sin\theta), \quad Y_m(3,6) = Y_m(3,5) \\
Y_m(4,1) &= Y_m(4,2) = \frac{jb_1\alpha_m}{k_1^2}, \quad Y_m(4,3) = Y_m(4,4) = \frac{jb_2\alpha_m}{k_2^2} \\
Y_m(4,5) &= -\frac{jg}{k_3^2\gamma_{3,m}}[(\gamma_{3,m}^2 + \beta^2)\cos\theta - \alpha_m\beta\sin\theta], \quad Y_m(4,6) = -Y_m(4,5) \\
Y_m(5,1) &= Y_m(5,2) = \frac{jb_1\beta}{k_1^2}, \quad Y_m(5,3) = Y_m(5,4) = \frac{jb_2\beta}{k_2^2} \\
Y_m(5,5) &= -\frac{jg}{k_3^2\gamma_{3,m}}[(\gamma_{3,m}^2 + \alpha_m^2)\sin\theta - \alpha_m\beta\cos\theta], \quad Y_m(5,6) = -Y_m(5,5) \\
Y_m(6,1) &= \frac{jb_1\gamma_{1,m}}{k_1^2}, \quad Y_m(6,2) = -Y_m(6,1) \\
Y_m(6,3) &= \frac{jb_2\gamma_{2,m}}{k_2^2}, \quad Y_m(6,4) = -Y_m(6,3) \\
Y_m(6,5) &= \frac{jg}{k_3^2}(\alpha_m\cos\theta + \beta\sin\theta), \quad Y_m(6,6) = Y_m(6,5)
\end{aligned}$$

here  $b_1 = a_1 - a_2k_1^2$ ,  $b_2 = a_1 - a_2k_2^2$ ; while

$$\begin{cases} \cos\theta = -\alpha_m/\sqrt{\alpha_m^2 + \beta^2}, \quad \sin\theta = -\beta/\sqrt{\alpha_m^2 + \beta^2}, & \text{if } \alpha_m^2 + \beta^2 \neq 0 \\ \cos\theta = \text{Inf}, \quad \sin\theta = \text{Inf}, & \text{if } \alpha_m^2 + \beta^2 = 0 \end{cases}$$

here Inf can be chosen as a very big number (e.g. Inf =  $10^{500}$ ), as at normal incidence ( $\alpha_m^2 + \beta^2 = 0$ ) no shear wave is excited [38],  $C_5^m = C_6^m = 0$  for all  $m \in [-\hat{m}, \hat{m}]$ .

## Appendix B. Derivation of the double summation identity Eq.(27)

The basic idea to prove the identity is to use  $e^{-jk_x^m x} e^{j2\pi n x/l_x} = e^{-jk_x^{(m-n)} x}$ , as  $k_x^m = k_x + 2m\pi/l_x$ . Then the left hand side of the identity becomes

$$\sum_{n=-\infty}^{+\infty} \left( \dots + W_{-1} e^{-jk_x^{-1-n} x} + W_0 e^{-jk_x^{-n} x} + W_1 e^{-jk_x^{1-n} x} + \dots \right) \quad (\text{B.1})$$

As the summation index  $n \in [-\infty, +\infty]$  in Eq.(B.1), if the summation is expanded and index  $n$  loops over  $n-1$  to  $n+1$ , then Eq.(B.1) becomes

$$\begin{aligned} & \left\{ \dots + \left( \dots + W_{-1} e^{-jk_x^{-n} x} + W_0 e^{-jk_x^{-n+1} x} + W_1 e^{-jk_x^{-n+2} x} + \dots \right) + \right. \\ & + \left( \dots + W_{-1} e^{-jk_x^{-n-1} x} + W_0 e^{-jk_x^{-n} x} + W_1 e^{-jk_x^{-n+1} x} + \dots \right) + \\ & \left. + \left( \dots + W_{-1} e^{-jk_x^{-n-2} x} + W_0 e^{-jk_x^{-n-1} x} + W_1 e^{-jk_x^{-n} x} + \dots \right) + \dots \right\} \end{aligned} \quad (\text{B.2})$$

If the terms with  $e^{-jk_x^{-n} x}$ ,  $e^{-jk_x^{-n+1} x}$ ,  $e^{-jk_x^{-n+2} x}$  ... in Eq.(B.2) were collected one by one, Eq.(B.2) becomes

$$\begin{aligned} & \left\{ \dots + e^{-jk_x^{-n} x} (\dots + W_{-1} + W_0 + W_1 + \dots) + \dots \right. \\ & + e^{-jk_x^{-n+1} x} (\dots + W_0 + W_1 + W_2 + \dots) + \dots \\ & \left. + e^{-jk_x^{-n+2} x} (\dots + W_1 + W_2 + W_3 + \dots) + \dots \right\} \end{aligned} \quad (\text{B.3})$$

Then the double summation identity Eq.(27) is obtained

$$\sum_{n=-\infty}^{+\infty} \sum_{m=-\infty}^{+\infty} W_m e^{-jk_x^m x} e^{j2\pi n x/l_x} = \sum_{n=-\infty}^{+\infty} W_n \sum_{m=-\infty}^{+\infty} e^{-jk_x^m x} \quad (\text{B.4})$$

## Appendix C. The elements of matrices in Eq.(28)

To be brief, here  $k_x^m$ ,  $k_y^m$ ,  $k_{i,z}^m$ ,  $k_{1,z}^m$ ,  $k_{2,z}^m$ ,  $k_{3,z}^m$  and  $k_{t,z}^m$  are replaced by  $\alpha_m$ ,  $\beta$ ,  $\gamma_{i,m}$ ,  $\gamma_{1,m}$ ,  $\gamma_{2,m}$ ,  $\gamma_{3,m}$  and  $\gamma_{t,m}$  respectively, and denote  $L_1 = h_1 + h_p$ ,  $L_2 = h_1 + h_p + h_2/2$ ,

$L_3 = h_1 + h_p + h_2$ , then the elements of matrix  $\mathbf{A}_m$  can be deduced as

$$\begin{aligned}
A_m(1, 9) &= j\omega, \quad A_m(1, 13) = j\gamma_{i,m} \\
A_m(2, 1) &= 2\frac{N\gamma_{1,m}\alpha_m}{k_1^2}e^{-jh_1\gamma_{1,m}/2}, \quad A_m(2, 2) = -2\frac{N\gamma_{1,m}\alpha_m}{k_1^2}e^{jh_1\gamma_{1,m}/2} \\
A_m(2, 3) &= 2\frac{N\gamma_{2,m}\alpha_m}{k_2^2}e^{-jh_1\gamma_{2,m}/2}, \quad A_m(2, 4) = -2\frac{N\gamma_{2,m}\alpha_m}{k_2^2}e^{jh_1\gamma_{2,m}/2} \\
A_m(2, 5) &= -\frac{Ne^{-jh_1\gamma_{3,m}/2}}{k_3^2} [(\beta^2 + \gamma_{3,m}^2 - \alpha_m^2)\cos\theta - 2\beta\alpha_m\sin\theta] \\
A_m(2, 6) &= -\frac{Ne^{jh_1\gamma_{3,m}/2}}{k_3^2} [(\beta^2 + \gamma_{3,m}^2 - \alpha_m^2)\cos\theta - 2\beta\alpha_m\sin\theta] \\
A_m(2, 7) &= -\frac{1}{2}(1 - \nu_p)D_{p1}\beta^2 + m_{s1}\omega^2 - D_{p1}\alpha_m^2 \\
A_m(2, 8) &= -\frac{1}{2}(1 + \nu_p)D_{p1}\beta\alpha_m \\
A_m(3, 1) &= [A + Q + b_1E_f + 2N\frac{\gamma_{1,m}^2}{k_1^2} - jh_1N\gamma_{1,m}\frac{\alpha_m^2 + \beta^2}{k_1^2}]e^{-jh_1\gamma_{1,m}/2} \\
A_m(3, 2) &= [A + Q + b_1E_f + 2N\frac{\gamma_{1,m}^2}{k_1^2} + jh_1N\gamma_{1,m}\frac{\alpha_m^2 + \beta^2}{k_1^2}]e^{jh_1\gamma_{1,m}/2} \\
A_m(3, 3) &= [A + Q + b_2E_f + 2N\frac{\gamma_{2,m}^2}{k_2^2} - jh_1N\gamma_{2,m}\frac{\alpha_m^2 + \beta^2}{k_2^2}]e^{-jh_1\gamma_{2,m}/2} \\
A_m(3, 4) &= [A + Q + b_2E_f + 2N\frac{\gamma_{2,m}^2}{k_2^2} + jh_1N\gamma_{2,m}\frac{\alpha_m^2 + \beta^2}{k_2^2}]e^{jh_1\gamma_{2,m}/2} \\
A_m(3, 5) &= -(\alpha_m\cos\theta + \beta\sin\theta) [(\alpha_m^2 + \beta^2)h_1 + 4j\gamma_{3,m} - h_1\gamma_{3,m}^2] \frac{jN}{2k_3^2}e^{-jh_1\gamma_{3,m}/2} \\
A_m(3, 6) &= -(\alpha_m\cos\theta + \beta\sin\theta) [(\alpha_m^2 + \beta^2)h_1 - 4j\gamma_{3,m} - h_1\gamma_{3,m}^2] \frac{jN}{2k_3^2}e^{jh_1\gamma_{3,m}/2} \\
A_m(3, 9) &= -D_1\alpha_m^4 - 2D_1\alpha_m^2\beta^2 - D_1\beta^4 + m_{s1}\omega^2, \quad A_m(3, 13) = j\rho_i\omega e^{jh_1\gamma_{i,m}/2} \\
A_m(4, 1) &= \frac{j\gamma_{1,m}}{k_1^2}e^{-jh_1\gamma_{1,m}}, \quad A_m(4, 2) = -\frac{j\gamma_{1,m}}{k_1^2}e^{jh_1\gamma_{1,m}} \\
A_m(4, 3) &= \frac{j\gamma_{2,m}}{k_2^2}e^{-jh_1\gamma_{2,m}}, \quad A_m(4, 4) = -\frac{j\gamma_{2,m}}{k_2^2}e^{jh_1\gamma_{2,m}}
\end{aligned}$$

$$\begin{aligned}
A_m(4, 5) &= (\alpha_m \cos \theta + \beta \sin \theta) \frac{j e^{-jh_1 \gamma_{3,m}}}{k_3^2} \\
A_m(4, 6) &= (\alpha_m \cos \theta + \beta \sin \theta) \frac{j e^{jh_1 \gamma_{3,m}}}{k_3^2} \\
A_m(4, 9) &= -1, \quad A_m(5, 1) = \frac{j b_1 \gamma_{1,m}}{k_1^2} e^{-jh_1 \gamma_{1,m}} \\
A_m(5, 2) &= -\frac{j b_1 \gamma_{1,m}}{k_1^2} e^{jh_1 \gamma_{1,m}} \\
A_m(5, 3) &= \frac{j b_2 \gamma_{2,m}}{k_2^2} e^{-jh_1 \gamma_{2,m}} \\
A_m(5, 4) &= -\frac{j b_2 \gamma_{2,m}}{k_2^2} e^{jh_1 \gamma_{2,m}}, \quad A_m(5, 5) = (\alpha_m \cos \theta + \beta \sin \theta) \frac{j e^{-jh_1 \gamma_{3,m}}}{k_3^2} \\
A_m(5, 6) &= (\alpha_m \cos \theta + \beta \sin \theta) \frac{j e^{jh_1 \gamma_{3,m}}}{k_3^2}, \quad A_m(5, 9) = -1 \\
A_m(6, 1) &= \frac{j \alpha_m}{k_1^2} e^{-jh_1 \gamma_{1,m}}, \quad A_m(6, 2) = \frac{j \alpha_m}{k_1^2} e^{jh_1 \gamma_{1,m}} \\
A_m(6, 3) &= \frac{j \alpha_m}{k_2^2} e^{-jh_1 \gamma_{2,m}}, \quad A_m(6, 4) = \frac{j \alpha_m}{k_2^2} e^{jh_1 \gamma_{2,m}} \\
A_m(6, 5) &= -\frac{j e^{-jh_1 \gamma_{3,m}}}{k_3^2 \gamma_{3,m}} [\gamma_{3,m}^2 \cos \theta + \beta (\beta \cos \theta - \alpha_m \sin \theta)] \\
A_m(6, 6) &= \frac{j e^{jh_1 \gamma_{3,m}}}{k_3^2 \gamma_{3,m}} [\gamma_{3,m}^2 \cos \theta + \beta (\beta \cos \theta - \alpha_m \sin \theta)] \\
A_m(6, 7) &= -1, \quad A_m(6, 9) = -\frac{1}{2} j h_1 \alpha_m \\
A_m(7, 1) &= \frac{j \beta}{k_1^2} e^{-jh_1 \gamma_{1,m}}, \quad A_m(7, 2) = \frac{j \beta}{k_1^2} e^{jh_1 \gamma_{1,m}} \\
A_m(7, 3) &= \frac{j \beta}{k_2^2} e^{-jh_1 \gamma_{2,m}}, \quad A_m(7, 4) = \frac{j \beta}{k_2^2} e^{jh_1 \gamma_{2,m}} \\
A_m(7, 5) &= -\frac{j e^{-jh_1 \gamma_{3,m}}}{k_3^2 \gamma_{3,m}} [\gamma_{3,m}^2 \sin \theta + \alpha_m (\alpha_m \sin \theta - \beta \cos \theta)] \\
A_m(7, 6) &= \frac{j e^{jh_1 \gamma_{3,m}}}{k_3^2 \gamma_{3,m}} [\gamma_{3,m}^2 \sin \theta + \alpha_m (\alpha_m \sin \theta - \beta \cos \theta)] \\
A_m(7, 8) &= -1, \quad A_m(7, 9) = -\frac{1}{2} j h_1 \beta \\
A_m(8, 1) &= \frac{j \gamma_{1,m}}{k_1^2} e^{-j L_1 \gamma_{1,m}}, \quad A_m(8, 2) = -\frac{j \gamma_{1,m}}{k_1^2} e^{j L_1 \gamma_{1,m}} \\
A_m(8, 3) &= \frac{j \gamma_{2,m}}{k_2^2} e^{-j L_1 \gamma_{2,m}}, \quad A_m(8, 4) = -\frac{j \gamma_{2,m}}{k_2^2} e^{j L_1 \gamma_{2,m}} \\
A_m(8, 5) &= \frac{j e^{-j L_1 \gamma_{3,m}}}{k_3^2} (\alpha_m \cos \theta + \beta \sin \theta)
\end{aligned}$$

$$\begin{aligned}
A_m(8, 6) &= \frac{j e^{j L_1 \gamma_{3,m}}}{k_3^2} (\alpha_m \cos \theta + \beta \sin \theta) \\
A_m(8, 12) &= -1, \quad A_m(9, 1) = \frac{j b_1 \gamma_{1,m}}{k_1^2} e^{-j L_1 \gamma_{1,m}} \\
A_m(9, 2) &= -\frac{j b_1 \gamma_{1,m}}{k_1^2} e^{j L_1 \gamma_{1,m}}, \quad A_m(9, 3) = \frac{j b_2 \gamma_{2,m}}{k_2^2} e^{-j L_1 \gamma_{2,m}} \\
A_m(9, 4) &= -\frac{j b_2 \gamma_{2,m}}{k_2^2} e^{j L_1 \gamma_{2,m}} \\
A_m(9, 5) &= \frac{j g e^{-j L_1 \gamma_{3,m}}}{k_3^2} (\alpha_m \cos \theta + \beta \sin \theta) \\
A_m(9, 6) &= \frac{j g e^{j L_1 \gamma_{3,m}}}{k_3^2} (\alpha_m \cos \theta + \beta \sin \theta) \\
A_m(9, 12) &= -1, \quad A_m(10, 1) = \frac{j \alpha_m}{k_1^2} e^{-j L_1 \gamma_{1,m}} \\
A_m(10, 2) &= \frac{j \alpha_m}{k_1^2} e^{j L_1 \gamma_{1,m}}, \quad A_m(10, 3) = \frac{j \alpha_m}{k_2^2} e^{-j L_1 \gamma_{2,m}} \\
A_m(10, 4) &= \frac{j \alpha_m}{k_2^2} e^{j L_1 \gamma_{2,m}} \\
A_m(10, 5) &= -\frac{j e^{-j L_1 \gamma_{3,m}}}{k_3^2 \gamma_{3,m}} [\gamma_{3,m}^2 \cos \theta + \beta (\beta \cos \theta - \alpha_m \sin \theta)] \\
A_m(10, 6) &= \frac{j e^{j L_1 \gamma_{3,m}}}{k_3^2 \gamma_{3,m}} [\gamma_{3,m}^2 \cos \theta + \beta (\beta \cos \theta - \alpha_m \sin \theta)] \\
A_m(10, 10) &= -1, \quad A_m(10, 12) = \frac{1}{2} j h_2 \alpha_m \\
A_m(11, 1) &= \frac{j \beta}{k_1^2} e^{-j L_1 \gamma_{1,m}}, \quad A_m(11, 2) = \frac{j \beta}{k_1^2} e^{j L_1 \gamma_{1,m}} \\
A_m(11, 3) &= \frac{j \beta}{k_2^2} e^{-j L_1 \gamma_{2,m}}, \quad A_m(11, 4) = \frac{j \beta}{k_2^2} e^{j L_1 \gamma_{2,m}} \\
A_m(11, 5) &= -\frac{j e^{-j L_1 \gamma_{3,m}}}{k_3^2 \gamma_{3,m}} [\gamma_{3,m}^2 \sin \theta + \alpha_m (\alpha_m \sin \theta - \beta \cos \theta)] \\
A_m(11, 6) &= \frac{j e^{j L_1 \gamma_{3,m}}}{k_3^2 \gamma_{3,m}} [\gamma_{3,m}^2 \sin \theta + \alpha_m (\alpha_m \sin \theta - \beta \cos \theta)] \\
A_m(11, 11) &= -1, \quad A_m(11, 12) = \frac{1}{2} j h_2 \beta \\
A_m(12, 1) &= -\frac{2N \alpha_m \gamma_{1,m}}{k_1^2} e^{-j L_2 \gamma_{1,m}}, \quad A_m(12, 2) = \frac{2N \alpha_m \gamma_{1,m}}{k_1^2} e^{j L_2 \gamma_{1,m}} \\
A_m(12, 3) &= -\frac{2N \alpha_m \gamma_{2,m}}{k_2^2} e^{-j L_2 \gamma_{2,m}}, \quad A_m(12, 4) = \frac{2N \alpha_m \gamma_{2,m}}{k_2^2} e^{j L_2 \gamma_{2,m}} \\
A_m(12, 5) &= \frac{N e^{-j L_2 \gamma_{3,m}}}{k_3^2} [(\gamma_{3,m}^2 + \beta^2 - \alpha_m^2) \cos \theta - 2 \alpha_m \beta \sin \theta]
\end{aligned}$$

$$\begin{aligned}
A_m(12, 6) &= \frac{N e^{jL_2 \gamma_{3,m}}}{k_3^2} [(\gamma_{3,m}^2 + \beta^2 - \alpha_m^2) \cos \theta - 2\alpha_m \beta \sin \theta] \\
A_m(12, 10) &= -\frac{1}{2} D_{p2} (1 - \nu_p) \beta^2 + m_{s2} \omega^2 - D_{p2} \alpha_m^2 \\
A_m(12, 11) &= -\frac{1}{2} D_{p2} (1 + \nu_p) \alpha_m \beta \\
A_m(13, 1) &= -[A + Q + b_1 E_f + 2N \frac{\gamma_{1,m}^2}{k_1^2} + j h_2 N \gamma_{1,m} \frac{\alpha_m^2 + \beta^2}{k_1^2}] e^{-jL_2 \gamma_{1,m}} \\
A_m(13, 2) &= -[A + Q + b_1 E_f + 2N \frac{\gamma_{1,m}^2}{k_1^2} - j h_2 N \gamma_{1,m} \frac{\alpha_m^2 + \beta^2}{k_1^2}] e^{jL_2 \gamma_{1,m}} \\
A_m(13, 3) &= -[A + Q + b_2 E_f + 2N \frac{\gamma_{2,m}^2}{k_2^2} + j h_2 N \gamma_{2,m} \frac{\alpha_m^2 + \beta^2}{k_2^2}] e^{-jL_2 \gamma_{2,m}} \\
A_m(13, 4) &= -[A + Q + b_2 E_f + 2N \frac{\gamma_{2,m}^2}{k_2^2} - j h_2 N \gamma_{2,m} \frac{\alpha_m^2 + \beta^2}{k_2^2}] e^{jL_2 \gamma_{2,m}} \\
A_m(13, 5) &= -(\alpha_m \cos \theta + \beta \sin \theta) [(\alpha_m^2 + \beta^2) h_2 - 4j \gamma_{3,m} - h_2 \gamma_{3,m}^2] \frac{jN}{2k_3^2} e^{-jL_2 \gamma_{3,m}} \\
A_m(13, 6) &= -(\alpha_m \cos \theta + \beta \sin \theta) [(\alpha_m^2 + \beta^2) h_2 + 4j \gamma_{3,m} - h_2 \gamma_{3,m}^2] \frac{jN}{2k_3^2} e^{jL_2 \gamma_{3,m}} \\
A_m(13, 12) &= -D_2 \alpha_m^4 - 2D_2 \alpha_m^2 \beta^2 - D_2 \beta^4 + m_{s2} \omega^2 \\
A_m(13, 14) &= -j \rho_t \omega e^{-jL_2 \gamma_{t,m}}, \quad A_m(14, 12) = j \omega \\
A_m(14, 14) &= -j \gamma_{t,m} e^{-jL_3 \gamma_{t,m}}
\end{aligned}$$

here  $D_{pi}$  is the in-plane stiffness,  $D_i$  is the bending stiffness,  $m_{si}$  is the surface density,  $i = 1, 2$  for the incident and transmitted side respectively; definition of  $\theta$  is given in [Appendix A](#); all the other elements in matrix  $\mathbf{A}_m$  are zero.

The non-zero element of matrix  $\mathbf{B}_n$  is  $B_n(13, 12) = K_z/l_x + K_y \alpha_n^2/l_x$ . The non-zero elements in vector  $\mathbf{p}$  are  $p(1) = jk_z$  and  $p(3) = -j \rho_i \omega e^{-jh_1 k_z/2}$ .

## References

- [1] F. X. Xin, T. J. Lu, C. Q. Chen, External mean flow influence on noise transmission through double-leaf aeroelastic plates, *AIAA J.* 47 (2009) 1939–1951.
- [2] K. Sakagami, M. Kiyama, M. Morimoto, Acoustic properties of double-leaf membranes with a permeable leaf on sound incidence side, *Appl. Acoust.* 63 (2002) 911 – 926.
- [3] B. H. Sharp, Prediction methods for the sound transmission of building elements, *Noise Control Eng.* 11 (1978) 53–63(11).
- [4] Q. Gu, J. Wang, Effect of resilient connection on sound transmission loss of metal stud double panel partitions, *Chin. J. Acoust.* (1983) 113–126.
- [5] J. L. Davy, Predicting the sound insulation of walls, *Build. Acoust.* 16 (2009) 1–20.
- [6] V. Hongisto, Sound insulation of double panels - comparison of existing prediction models, *Acta Acust. United Ac.* 92 (2006) 61–78.
- [7] J. Legault, N. Atalla, Numerical and experimental investigation of the effect of structural links on the sound transmission of a lightweight double panel structure, *J. Sound Vib.* 324 (2009) 712 – 732.
- [8] M. A. Biot, Theory of propagation of elastic waves in a fluid-saturated porous solid. i. low-frequency range, *J. Acoust. Soc. Am.* 28 (1956) 168–178.
- [9] J. Allard, Y. Champoux, New empirical equations for sound propagation in rigid frame fibrous materials, *J. Acoust. Soc. Am.* 91 (1992) 3346–3353.

- [10] A. Trochidis, A. Kalaroutis, Sound transmission through double partitions with cavity absorption, *J. Sound Vib.* 107 (1986) 321 – 327.
- [11] F. Xin, T. Lu, Sound radiation of orthogonally rib-stiffened sandwich structures with cavity absorption, *Compos. Sci. Technol.* 70 (2010) 2198 – 2206.
- [12] Y. Liu, C. He, Diffuse field sound transmission through sandwich composite cylindrical shells with poroelastic core and external mean flow, *Compos. Struct.* 135 (2016) 383 – 396.
- [13] J.-H. Lee, J. Kim, H.-J. Kim, Simplified method to solve sound transmission through structures lined with elastic porous material, *J. Acoust. Soc. Am.* 110 (2001) 2282–2294.
- [14] J. Legault, N. Atalla, Sound transmission through a double panel structure periodically coupled with vibration insulators, *J. Sound Vib.* 329 (2010) 3082 – 3100.
- [15] J. Bolton, N.-M. Shiau, Y. Kang, Sound transmission through multi-panel structures lined with elastic porous materials, *J. Sound Vib.* 191 (1996) 317 – 347.
- [16] H. Deresiewicz, J. T. Rice, The effect of boundaries on wave propagation in a liquid-filled porous solid: iii. reflection of plane waves at a free plane boundary (general case), *Bull. Seismol. Soc. Am.* 52 (1962) 595–625.
- [17] J. F. Allard, C. Depollier, P. Rebillard, W. Lauriks, A. Cops, Inhomogeneous Biot waves in layered media, *J. Appl. Phys.* 66 (1989) 2278–2284.
- [18] J. Zhou, A. Bhaskar, X. Zhang, Sound transmission through a double-panel construction lined with poroelastic material in the presence of mean flow, *J. Sound Vib.* 332 (2013) 3724 – 3734.
- [19] Y. Liu, A. Sebastian, Effects of external and gap mean flows on sound transmission through a double-wall sandwich panel, *J. Sound Vib.* 344 (2015) 399 – 415.
- [20] L. Alimonti, N. Atalla, A. Berry, F. Sgard, A hybrid finite element-transfer matrix model for vibroacoustic systems with flat and homogeneous acoustic treatments, *J. Acoust. Soc. Am.* 137 (2015) 976–988.
- [21] D. Mead, K. Pujara, Space-harmonic analysis of periodically supported beams: response to convected random loading, *J. Sound Vib.* 14 (1971) 525 – 541.
- [22] F. Xin, T. Lu, Analytical modeling of fluid loaded orthogonally rib-stiffened sandwich structures: sound transmission, *J. Mech. Phys. Solids* 58 (2010) 1374 – 1396.
- [23] J. Legault, A. Mejdji, N. Atalla, Vibro-acoustic response of orthogonally stiffened panels: the effects of finite dimensions, *J. Sound Vib.* 330 (2011) 5928 – 5948.
- [24] B. Mace, Periodically stiffened fluid-loaded plates, i: response to convected harmonic pressure and free wave propagation, *J. Sound Vib.* 73 (1980) 473 – 486.
- [25] G. Lin, J. M. Garrelick, Sound transmission through periodically framed parallel plates, *J. Acoust. Soc. Am.* 61 (1977) 1014–1018.
- [26] J. Brunskog, The influence of finite cavities on the sound insulation of double-plate structures, *J. Acoust. Soc. Am.* 117 (2005) 3727–3739.
- [27] H. Chung, G. Emms, Fourier series solutions to the vibration of rectangular lightweight floor/ceiling structures, *Acta Acust. United Ac.* 94 (2008) 401–409.
- [28] J. Brunskog, H. Chung, Non-diffuseness of vibration fields in ribbed plates, *J. Acoust. Soc. Am.* 129 (2011) 1336–1343.
- [29] K. A. Dickow, J. Brunskog, M. Ohlrich, Modal density and modal distribution of bending wave vibration fields in ribbed plates, *J. Acoust. Soc. Am.* 134 (2013) 2719–2729.
- [30] F. X. Xin, T. J. Lu, Analytical and experimental investigation on transmission loss of clamped double panels: implication of boundary effects, *J. Acoust. Soc. Am.* 125 (2009) 1506–1517.
- [31] Y. Liu, J.-C. Catalan, External mean flow influence on sound transmission through finite clamped double-wall sandwich panels, *J. Sound Vib.* 405 (2017) 269 – 286.
- [32] A. J. Hull, J. R. Welch, Elastic response of an acoustic coating on a rib-stiffened plate, *J. Sound Vib.* 329 (2010) 4192 – 4211.
- [33] B. Mace, Sound radiation from fluid loaded orthogonally stiffened plates, *J. Sound Vib.* 79 (1981) 439 – 452.
- [34] P. M. Morse, K. U. Ingard, *Theoretical Acoustics*, Princeton University Press, 1968.
- [35] F. Axisa, P. Trompette, *Modelling of Mechanical Systems*, volume 2, Butterworth-Heinemann, 2005.
- [36] M. C. Junger, D. Feit, *Sound, Structures, and Their Interaction*, MIT Press Cambridge, Ma, 1986.
- [37] S. S. Rao, *Vibration of Continuous Systems*, John Wiley & Sons, 2007.
- [38] J. F. Allard, N. Atalla, *Propagation of Sound in Porous Media*, John Wiley & Sons, Ltd, 2009.
- [39] K. F. Graff, *Wave Motion in Elastic Solids*, Ohio State University Press, 1975.
- [40] S. A. Hambric, S. H. Sung, D. J. Nefske, *Engineering Vibroacoustic Analysis: Methods and Applications*, John Wiley & Sons, 2016.